An equivalent method of jet impact loading from collapsing near-wall acoustic bubbles: A preliminary study

Xiang Lu [a,b], Chen Chen [a,b,*], Kai Dong [a,b,c], Zefa Li [a,b], Jiankang Chen [a,b]

[a] State Key Laboratory of Hydraulics and Mountain River Engineering, Sichuan University, No. 24 South Section 1, Yihuan Road, Chengdu 610065, China
[b] College of Water Resources & Hydropower, Sichuan University, No. 24 South Section 1, Yihuan Road, Chengdu 610065, China
[c] Department of Dam Safety Management, Nanjing Hydraulic Research Institute, No. 223 Guangzhou Road, Nanjing 210029, China

ARTICLE INFO

ABSTRACT

Cavitation damage is a micro, high-speed, multi-phase complex phenomenon caused by the near-wall bubble group collapse. The current numerical simulation method of cavitation mainly focuses on the collapse impact of a single cavitation bubble. The large-scale simulation of the cavitation bubble group collapse is difficult to perform and has not been studied, to the best of our knowledge. In this study, the equivalent model of impact loading of acoustic bubble collapse micro-jets is proposed to study the cavitation erosion damage of materials. Based on the theory of the micro-jet and the water hammer effect of the liquid–solid impact, an equivalent model of impact loading of a single acoustic bubble collapse micro-jet is established under the principle of deformation equivalence. Since the acoustic bubbles can be considered uniformly distributed in a small enough area, an equivalent model of impact loading of multiple acoustic bubble collapse micro-jets in a micro-segment can be derived based on the equivalent results of impact loading of a single acoustic bubble collapse micro-jet. In fact, the equivalent methods of cavitation damage loading for single and multiple near-wall acoustic bubble collapse micro-jets are formed. The verification results show the law of cavitation deformation of concrete using equivalent loading is consistent with that of a micro-jet simulation, and the average relative errors and the mean square errors are insignificant. The equivalent method of impact loading proposed in this paper has high accuracy and can greatly improve the calculation efficiency, which provides technical support for numerical simulation of concrete cavitation.

1. Introduction

Cavitation erosion is a micro, high-speed, and multi-phase complex phenomenon, and there are many theories about the mechanism of cavitation damage, such as mechanical action, thermal action, and chemical corrosion [1]. The discharge structures of dams are located in a complex environment with characteristics of high-water head, large discharge, and high flow rate, and cavitation damage of concrete structure is a common engineering problem during the operation period addressed by scholars and engineers.

Several research studies have focused on material cavitation. Cavitation erosion experiments and numerical simulation are the two main methods to study the cavitation performance of materials [2–5]. With respect to cavitation erosion experiments, the size and collapse process of a cavitation bubble and its damage on materials are widely investigated [6,7]. Philipp and Lauterborn [8] studied the dynamics of a single

cavitation bubble and the resulting surface damage on a flat metal specimen. They defined the relationship between the distance between the boundary and the bubble center at the moment of formation (s) and the maximum bubble radius (R_{max}) as $\gamma = s/R_{max}$. The authors concluded bubbles in the ranges $\gamma \leqslant 0.3$ and $\gamma = 1.2$ to 1.4 caused the greatest damage. Pan *et al.* [9] studied the erosion property of a self-excited cavitating jet produced by an organ-pipe nozzle. E *et al* [10] compared the cavitation erosion and slurry erosion resistance of different coating materials from the aspects of mass loss, erosion morphology, and roughness. Alturki *et al.* [11] used the wavelet transform method and fractal analysis to characterize the surface morphologies of stainless steel cavitated in water.

With respect to numerical simulations, many studies focus on the collapse of cavitation bubbles. For example, Zhang *et al.* [12] studied the conversion relationship between cavitation bubble potential energy and wave energy during the collapse of cavitation bubbles near the wall. Han
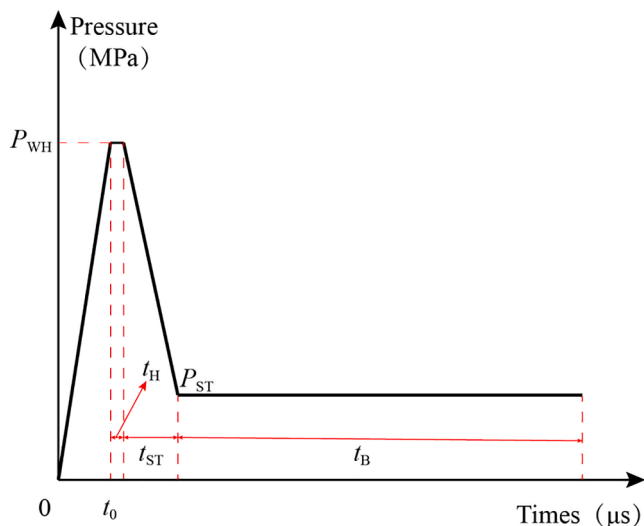

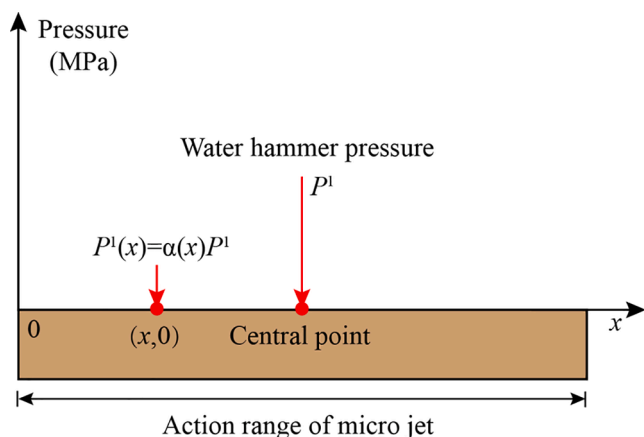**Fig. 1.** Pressure curve on the center of the solid wall caused by jet.

Fig. 2. Equivalent diagram of loading at different positions in the action area of a single micro-jet.
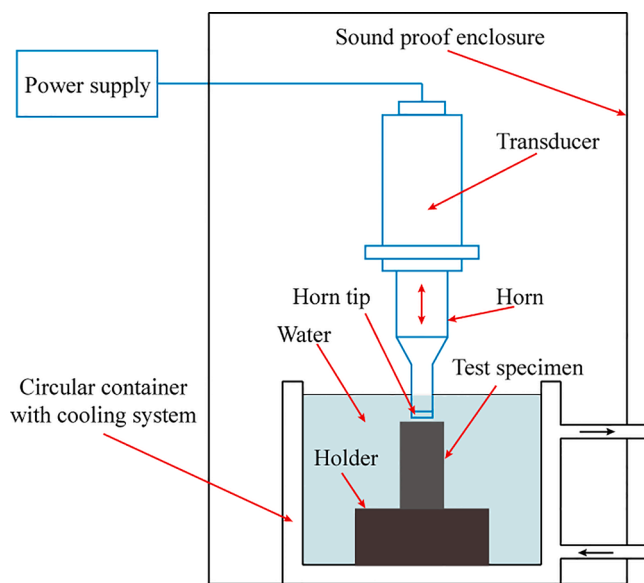

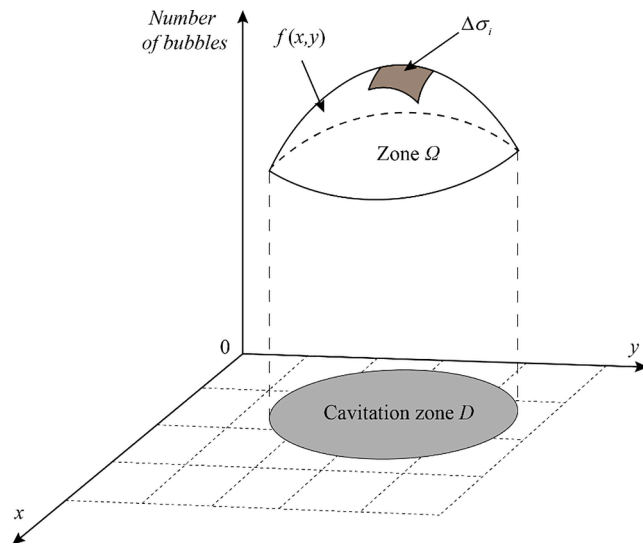**Fig. 3.** Diagram of the ultrasonic vibratory device.

Fig. 4. Characteristics assumption of a micro-area in the cavitation cloud structure.
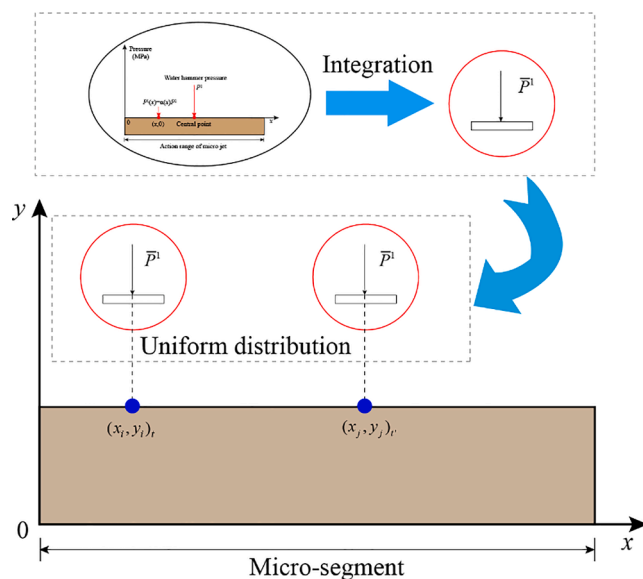

Fig. 5. Equivalent diagram of the impact from single micro-jet to multitype micro-jets.

et al. [13] established a three-dimensional numerical model to simulate the collapse process of cavitation in the free field by using mass conservation and momentum conservation for weakly compressible fluids. This study examined the energy conversion mechanism of the bubble in the collapse process. Generally, a large number of cavitation bubbles exist in the cavitation field, and the effect of collapse between cavitation bubbles is complex.

Presently, an adequate method for macroscopic numerical simulation of cavitation erosion requires development. Peters and Moctar [14] proposed a multi-scale Euler–Lagrange method based on the conversion mechanism of Eulerian vapor volumes into Lagrangian bubbles. Usta and Korkut [15] simulated the cavitation development for a hydrofoil and propeller by using the Schnerr–Sauer cavitation model to predict the amount of erosion through the intensity function method, gray level method, and erosive power method. Their approach determined the potential cavitation area of structures. Based on previous research, a
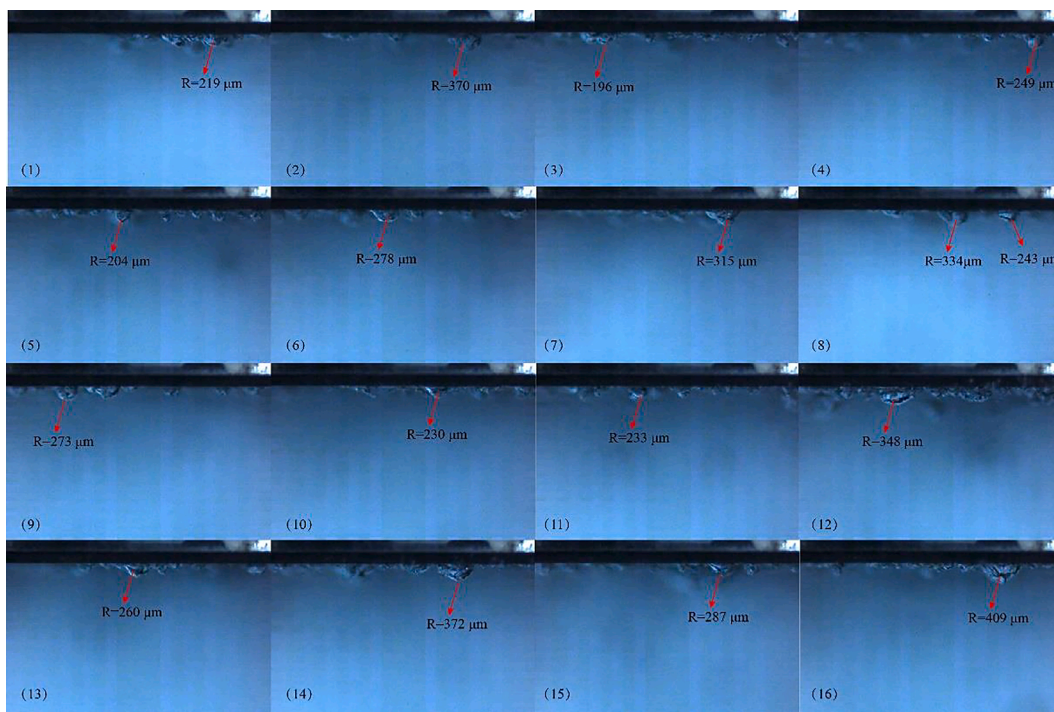
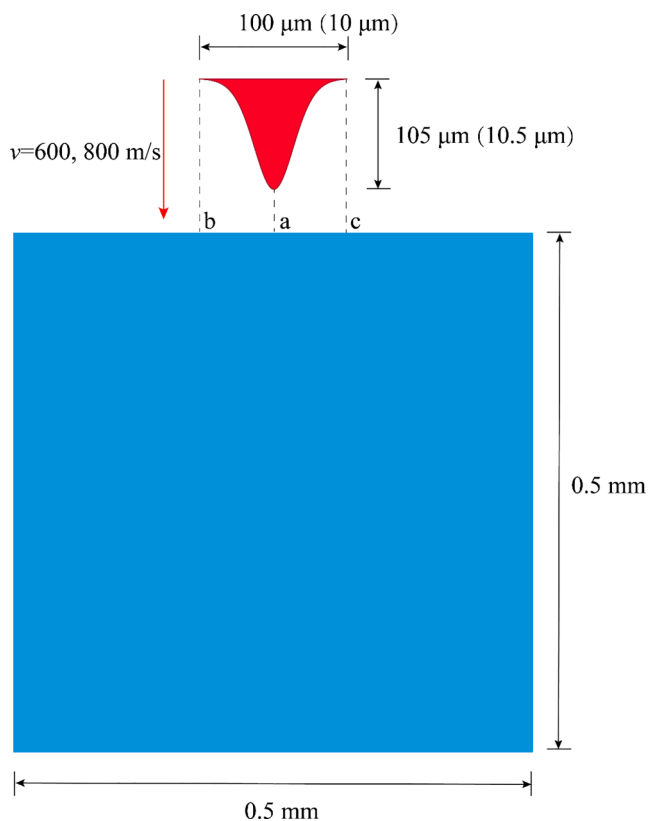**Fig. 6.** The size of cavitation bubbles and micro-jets generated by the ultrasonic vibratory device.

Fig. 7. The two-dimensional finite element model.

Table 1
Parameters in the model.

Materials	Density (kg·m^{-3})	Sound velocity (m·s^{-1})	Elastic modulus (GPa)	Compressive strength (MPa)	Poisson ratio
Water	1000	1500	/		
Concrete	2400	4000	41	30	0.20

Table 2
Plastic parameters of the CDP model.

$\psi/(°)$	$\in$	σ_{b0}/σ_{c0}	k_c	μ
30	0.1	1.16	0.6667	0.0005

Note: ψ is the dilation angle; $\in$ is the eccentricity; σ_{b0}/σ_{c0} is the ratio of the biaxial and uniaxial ultimate compressive strengths; k_c is the ratio of stress invariants; and μ is the viscosity parameter.

fluid–structure coupled model of near-wall acoustic cavitation bubble collapse micro-jet impact based on fluid mechanics and impact dynamics. The simulation results were in good agreement with the experimental results. Therefore, the micro-jet theory can be adopted to study the mechanism and the loading characteristics of cavitation erosion.

The equivalent loading method is commonly used in structural analysis, and it is widely used in the calculation and analysis of pre-stressed loading, wind loading, vehicle loading, and blasting loading [19–22]. Zhang *et al.* [23] derived the equivalent loading method of blasting vibration based on the equivalent principle of Saint-Venant loading. The results showed the equivalent loading method has the advantages of simple modeling, easy convergence, and good accuracy. Dong *et al.* [24] used the classical load-response correlation method to obtain the equivalent static wind loading vectors at different nodes of long-span bridges. These numerical analysis examples showed demonstrate the equivalent wind loading performs well in terms of calculation accuracy and rationality of loading distribution. Gao and Li [25]

macro-scale cavitation simulation still requires development. Additionally, the impact effect caused by cavitation collapse is the main reason for material cavitation erosion, and the cavitation erosion caused by micro-jet impact on the surface is one of the main mechanisms of the material cavitation effect [16,17]. Ye and Zhu [18] established a
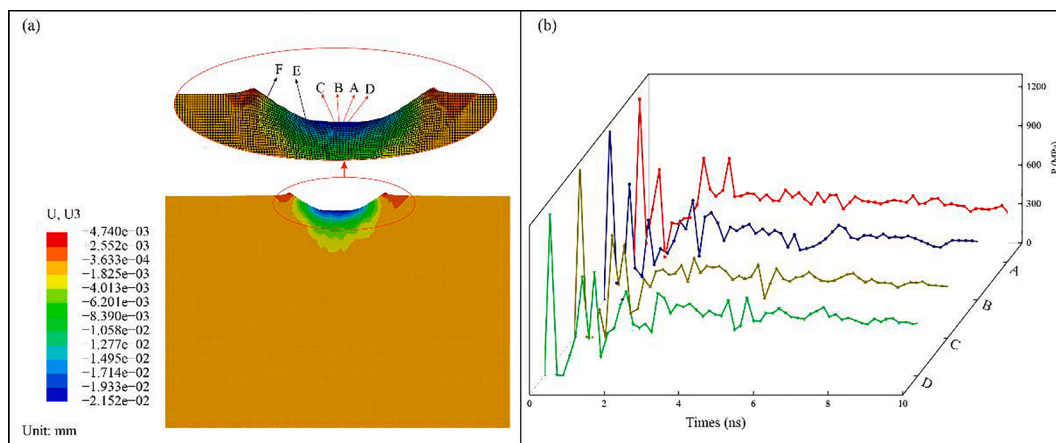
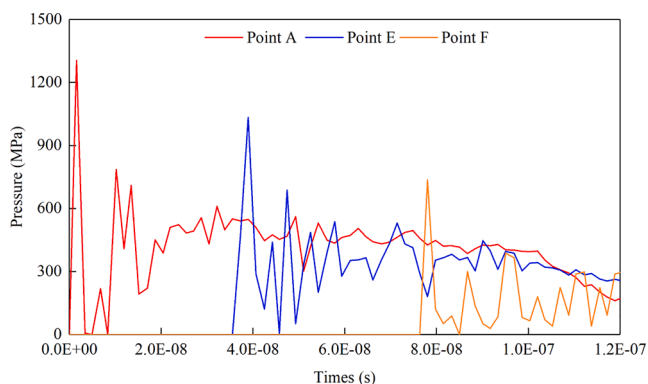**Fig. 8.** The node stress at the center of the impact loading.

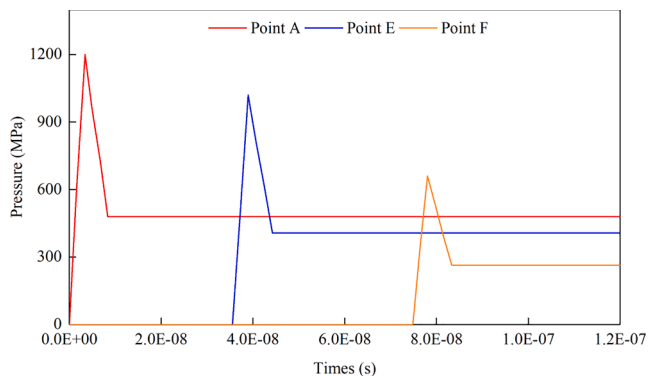**Fig. 9.** The comparison of pressure in different locations.

Fig. 10. The equivalent loading of a single micro-jet.

detailed the equivalent constant-amplitude cyclic loading method for random vehicle loading based on the principle of energy equivalence and established its accuracy and superiority. In the aspect of hydraulic concrete structure, Wang *et al.* [26] obtained the equivalent fluctuating load on each discharge flow outlet by using flow-induced vibration back analysis and studied the influence of fluctuating pressure on the dynamic response of an arch dam. Chen *et al.* [27] reported the equivalent loading method of uplift pressure of gravity dam using mechanical analysis, numerical simulation, and experimental investigation.

The purpose of this paper is to study the loading equivalent method of cavitation damage based on the micro-jet theory and explore the

loading equivalent method of single and multiple cavitation bubble collapse micro-jets impact. The main contents of this paper are as follows: (1) the basic theory of micro-jet and the coupled Eulerian–Lagrangian (CEL) method are introduced; (2) the equivalent method of loading of a single micro-jet is proposed based on the principle of water hammer; (3) the equivalent method of collapse impact of multiple micro-jets on the micro-segment is detailed based on the equivalent method of collapse impact loading of a single micro-jet; (4) based on a generalized model, the accuracy of the two equivalent methods is verified, and the direction of further research is discussed.

2. Methodology

2.1. CEL method

Compared with the traditional Lagrangian method and the Euler method, the CEL method can effectively overcome element distortion and achieve a high-precision material boundary capture [28]. It has advantages with respect to addressing large deformation problems such as liquid surface sloshing, collision, and fluid–solid coupling. The flow state of liquid is represented by fluid volume in the CEL method; it is determined according to the Eulerian volume fraction (EVF) of each Euler element. When EVF = 1, the element is filled with liquid, and when EVF = 0, the unit is not filled with liquid.

The governing equation of the CEL method consists of the continuity equation, the momentum conservation equation, and the energy conservation equation. They are expressed as Eqs. (1)–(3), respectively:

$$\frac{D\rho}{Dt} + \rho \nabla \nu = \frac{\partial \rho}{\partial t} + \nu \nabla \rho + \rho \nabla \nu = 0 \tag{1}$$

$$\rho \frac{D\nu}{Dt} = \nabla \boldsymbol{\sigma} + \rho \boldsymbol{b} \tag{2}$$

with $\frac{\mathrm{D}\nu}{\mathrm{D}t} = \frac{\partial \sigma}{\partial t} + \nu \nabla \nu$.

$$\rho \frac{\mathrm{D}E}{\mathrm{D}t} = \boldsymbol{\sigma} \dot{\varepsilon} + \rho \dot{Q} \tag{3}$$

with $\dot{\varepsilon} = \frac{1}{2}(\nabla \nu + \nabla \nu^{\mathrm{T}})$.

In Eqs. (1)–(3), ρ is the density of liquid, ∇ is the vector differential operator, ν is the vector of liquid velocity, $\boldsymbol{\sigma}$ is the tensor of Cauchy stress, $\boldsymbol{b}$ is the tensor of unit resultant force, E is the energy, $\dot{\varepsilon}$ is the strain rate, and $\dot{Q}$ is the thermal conductivity.

In the CEL method, the state equation of the Euler material is used to determine the functional relationship between the physical quantities such as the temperature, pressure, and energy of the material. The Euler material, in the context of this work, is water, so the state equation, $U_s - U_p$, is introduced, as Eq. (4) [29],
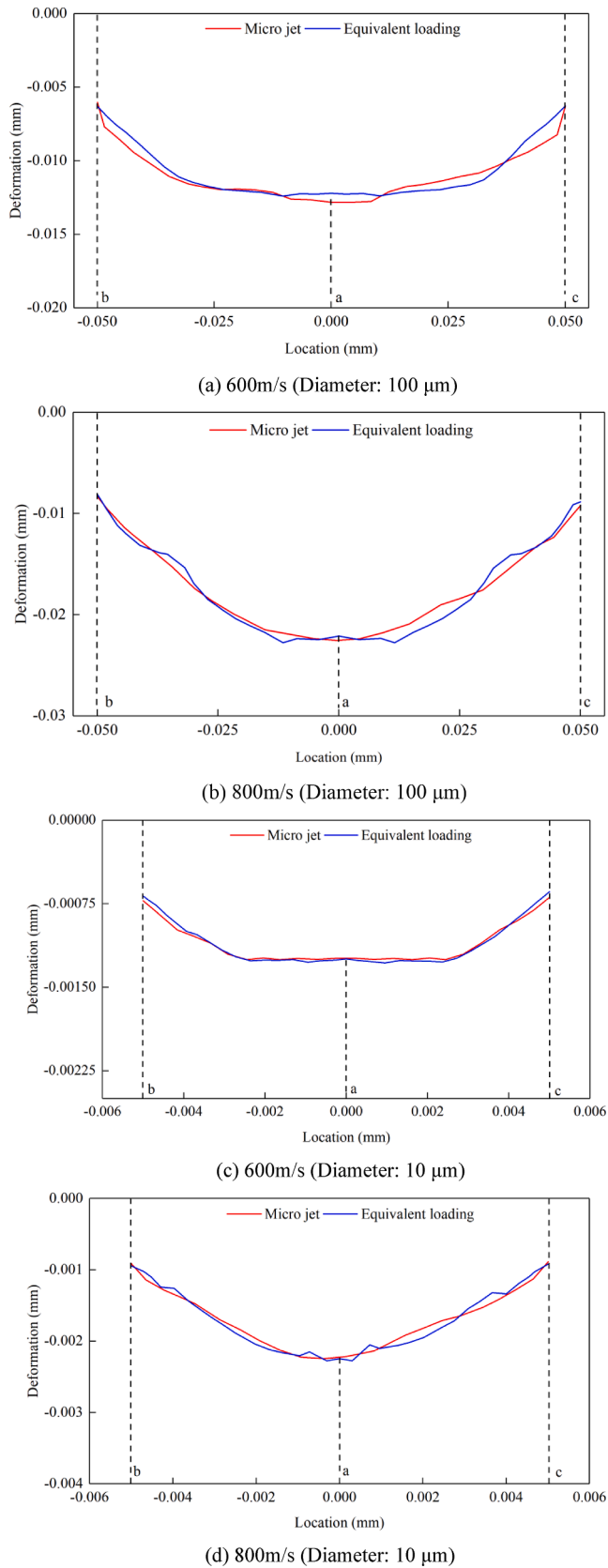
(a) 600m/s (Diameter: 100 μm)

(b) 800m/s (Diameter: 100 μm)

(c) 600m/s (Diameter: 10 μm)

(d) 800m/s (Diameter: 10 μm)

Fig. 11. Comparison of deformation results of a single micro-jet and equivalent loading.

Table 3
The average relative errors and MSE of the results.

Diameter (μm)	Velocity (m/s)	Evaluation indexes	
		δ (%)	MSE (mm)
100	800	3.83	7.08×10^{-4}
	600	4.91	5.79×10^{-4}
10	800	4.16	7.92×10^{-5}
	600	3.41	4.65×10^{-5}

$$P = \frac{\rho_0 c_0^2 \eta}{(1 - s\eta)^2}\left(1 - \frac{\Gamma_0 \eta}{2}\right) + \Gamma_0 \rho_0 E_m \tag{4}$$

where ρ_0 is the initial density of liquid, c_0 is the sound velocity of liquid, Γ_0 and s are the constants related to liquids, E_m is the internal energy per unit mass of liquid, and η is the nominal volume compression strain.

In addition, the general contact algorithm is selected for the liquid–solid contact algorithm in the CEL method, and the contact attribute is the hard contact.

2.2. Water hammer pressure

The water hammer pressure was first introduced by Cook [30] to explain the pressure caused by liquid–solid high-speed impact. Currently, it is widely used to describe the jet impact on a wall. When a solid surface is hit by a high-speed jet, the pressure at its central point is called "water hammer pressure," which can be calculated by Eq. (5) [31]:

$$P_{WH} = \rho_L c_L v\left(\frac{\rho_S c_S}{\rho_L c_L + \rho_S c_S}\right) \tag{5}$$

where P_{WH} is the water hammer pressure, ρ_L and ρ_S are the density of the liquid and solid, respectively, c_L and c_S are the speeds of which sound travels in liquid and solid, respectively, and v is the velocity of the micro-jet. Generally, the value of $\rho_S c_S$ is much greater than that of $\rho_L c_L$. As such, Eq. (5) can be approximately expressed as Eq. (6):

$$P_{WH} \approx \rho_L c_L v \tag{6}$$

During the process of jet impact, the time, t_H, of the water hammer pressure acting on the structure is very short. The impact time is expressed by

$$t_H = \frac{D}{2c_L} \tag{7}$$

where D is the diameter of the micro-jet.

After the water hammer pressure is released, the pressure at the impact center gradually attenuates until it enters the stage of pressure stagnation. At this time, the pressure P_{ST} and the attenuation time t_{ST} can be expressed as Eqs. (8)–(9) [32]:

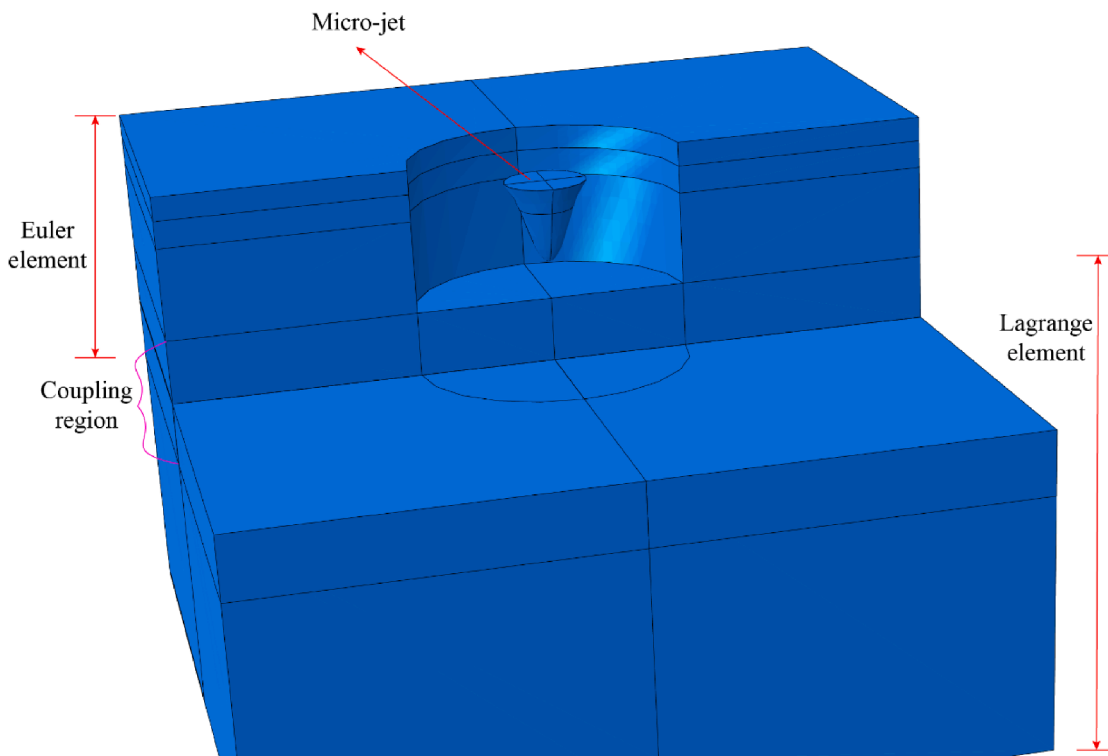$$P_{ST} = \frac{\rho_L v^2}{2} \tag{8}$$
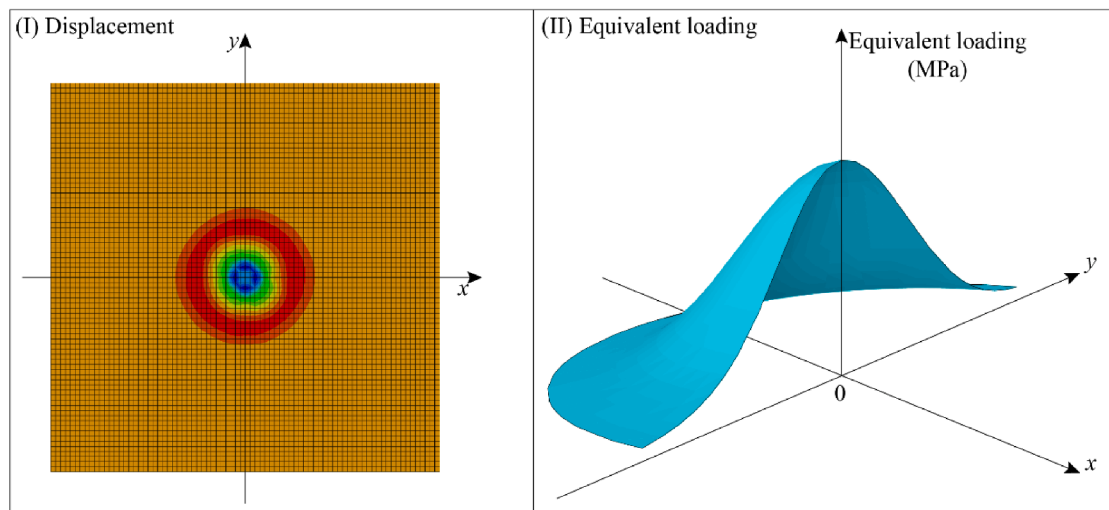
$$t_{ST} = \frac{3D}{2c_L} \tag{9}$$

During the stage of pressure stagnation, the duration, t_B, is relatively long, as evaluated by Eq. (10):

$$t_B = t_H + 2t_{ST} \tag{10}$$

Therefore, the water hammer pressure is used to describe the loading form of the jet impacting the solid surface, as shown in Fig. 1. The action

(a) The three-dimensional finite element model

(b) Displacement and equivalent loading

Fig. 12. The three-dimensional finite element model and its corresponding loading.

time of loading caused by the liquid–solid high-speed impact is susceptible to many factors, such as the liquid properties and the shape of micro-jet. Therefore, the values of the time nodes (t_H, t_{ST}, t_B) in Fig. 1 should be determined according to the stress process of the CEL simulation results. When the micro-jet model is used for the cavitation damage analysis, the total action time of micro-jet impact is the time when the top of the micro-jet moves to the solid surface, which agrees with previous studies [33,34].

2.3. Equivalent model of impact loading of a single acoustic bubble collapse

Based on the water hammer pressure, the pressure at the center of the micro-jet impact on the surface can be approximated by the curve in Fig. 1. However, as the loading is related to the jet shape, liquid characteristics, and simulation method, the relevant parameters of the impact water hammer pressure curve need to be determined in combination with the simulation results. The duration, t_H, of the water
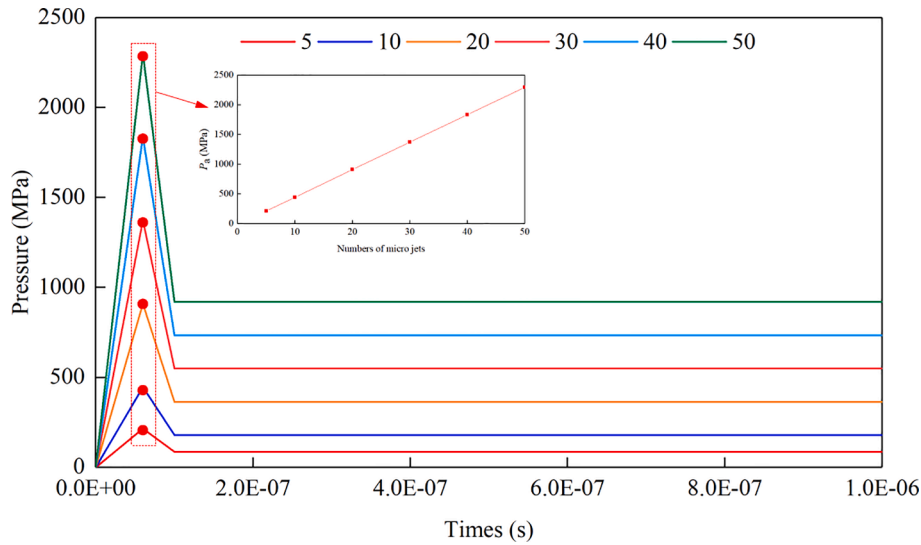
Fig. 13. Equivalent loading under different impact times of micro-jets.
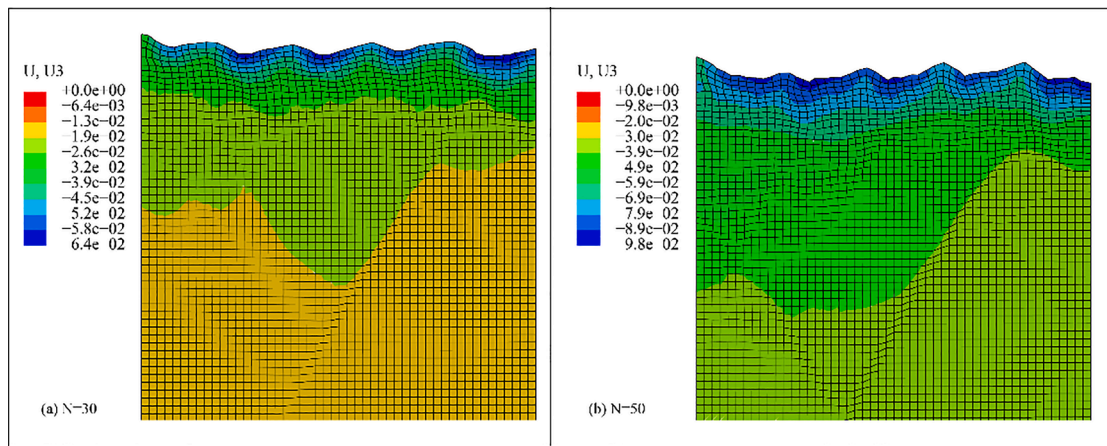

Fig. 14. Cloud chart of concrete deformation under the impact of multitype micro-jets (unit: mm).

hammer pressure is very short, so it does not require consideration in this simulation. Therefore, the loading at the center of the concrete surface impacted by a single micro-jet can be evaluated by Eq. (11):

$$
P^1 = \begin{cases} \dfrac{t}{t_0}P_{WH} & 0 \leqslant t \leqslant t_0 \\[2mm] \dfrac{P_{WH}(t_0 + t_{ST}) - P_{ST}t_0}{t_{ST}} & t_0 \leqslant t \leqslant t_0 + t_{ST} \\[2mm] P_{ST} & t \geqslant t_0 + t_{ST} \end{cases} \tag{11}
$$

where P^1 is the equivalent loading at the center of a single micro-jet impact.

The micro-jet has a certain volume, so the area of the micro-jet acting on the surface is an area loading. From the perspective of the mechanical mechanism for micro-jet impact, the loading forms of different positions in the interaction area between micro-jet and concrete are similar to the form of water hammer pressure. There is a difference in the extreme value, which is the largest in the middle and gradually decreases to both sides. Therefore, based on the loading equivalent calculation method of micro-jet impact center pressure, the equivalent loading at different positions within the action range of micro-jet can be expressed as Eq. (12),

$$
P^1(x) = \begin{cases} \dfrac{t}{t_0}\alpha(x)P_{WH} & 0 \leqslant t \leqslant t_0 \\[2mm] \alpha(x)\dfrac{P_{WH}(t_0 + t_{ST}) - P_{ST}t_0}{t_{ST}} & t_0 \leqslant t \leqslant t_0 + t_{ST} \\[2mm] \alpha(x)P_{ST} & t \geqslant t_0 + t_{ST} \end{cases} \tag{12}
$$

where $\alpha(x)$ is the attenuation coefficients at different positions. These coefficients can be determined by the inversion of micro-jet numerical simulation. To distinguish the equivalent loading under different scales, the symbol $\overline{P}^1$ is used to represent the equivalent loading of a single micro-jet impact. The equivalent loading as a function of position is illustrated in Fig. 2.

2.4. Equivalent model of impact loading of multiple acoustic bubbles collapse

Research shows the time of micro-jet impact ranges from 100 to 1000 / (s·cm^2) when the cavitation occurs on the solid surface [35]. The cavitation structure caused by the ultrasonic cavitation equipment (as seen in Fig. 3) is usually nonuniform and has strong randomness [36].
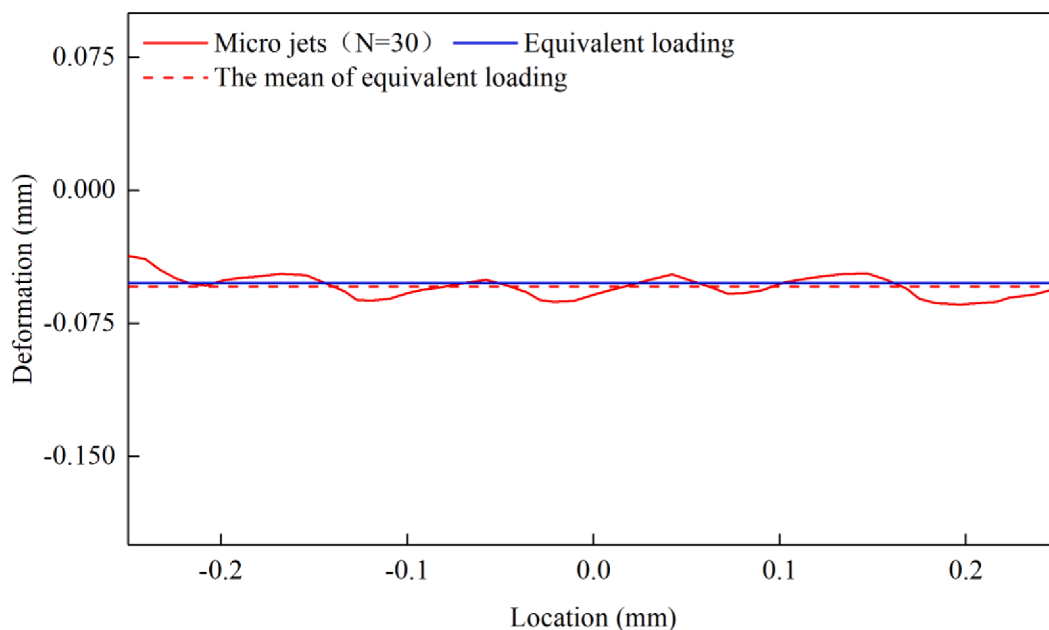
(a) N=30
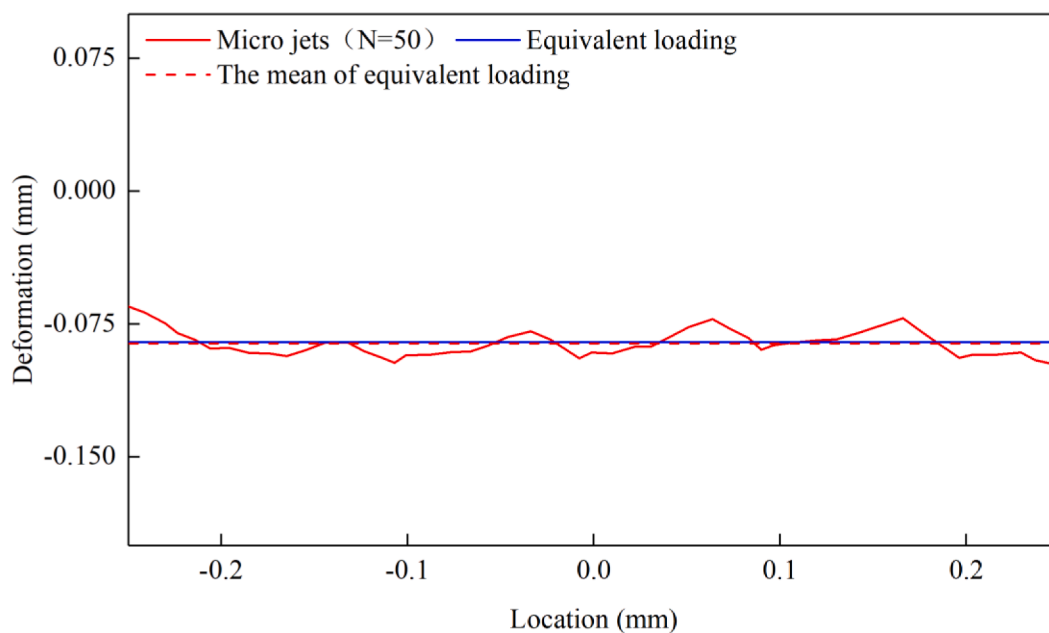
(b) N=50

Fig. 15. Comparison of deformation results of multiple micro-jets and equivalent loading.

Some necessary assumptions are utilized to study the equivalent loading of multiple acoustic bubbles collapse micro-jets.

The distribution of cavitation bubbles is random and continuous in space, so a function, $f(x, y)$, can be used to describe the number of bubbles in the cavitation zone, D, as shown in Fig. 4. The zone, Ω, of cavitation bubbles is divided into n micro-areas of $\Delta\sigma_1$, …, $\Delta\sigma_i$, …, $\Delta\sigma_n$. The change of the function values in the micro-area, $\Delta\sigma_i$, is very small because of the continuity of the function. $f(x, y)$, so the micro-curved surface of $\Delta\sigma_i$ can be approximately regarded as a micro-plane [37]. In addition, the distribution of cavitation bubbles in the micro-area of $\Delta\sigma_i$ is assumed to be uniform. These assumptions are widely used in the discretization and simulation of material and loading random fields of

civil engineering [38,39], so the assumptions mentioned above are reasonable.

Combined with the equivalent loading analysis method of a single micro-jet, the deformation response of concrete and loading form impacted by multiple micro-jets on the micro-segment in the two-dimensional space can be generalized, as shown in Fig. 5. Considering the micro-jet on the micro-segment is uniformly distributed, the impact loading on the micro-segment is also uniformly distributed when the impact velocity is consistent. Therefore, the multiple micro-jets impact loading on the micro-segment can be equivalent to a uniform impact loading, as expressed by Eq. (13),

$$\overline{P}^2 = f\left(N, \overline{P}^1\right) = f(N, v) = \begin{cases} \dfrac{t}{t_0}P_a & 0 \leqslant t \leqslant t_0 \\ \dfrac{P_a(t_0 + t_{ST}) - P_b t_0}{t_{ST}} & t_0 \leqslant t \leqslant t_0 + t_{ST} \\ P_b & t \geqslant t_{ST} \end{cases} \quad (13)$$

where $\overline{P}^2$ is the equivalent loading of concrete impacted by multiple micro-jets, which is a uniformly distributed impact loading. Moreover, in Eq. (13), N represents the number of microfluidic actions per unit time, v accounts for the velocity of the micro-jet, D equals the diameter of the micro-jet, and $f(\cdot)$ models the function form. Finally, P_a and P_b are loading values of the inflection points on the loading curve, which correspond to P_{WH} and P_{ST} in Fig. 1.

3. Accuracy verification

3.1. A single acoustic bubble collapse

3.1.1. Model and parameters

A two-dimensional model is selected to analyze the accuracy and the effectiveness of equivalent loading. At the later stage of the collapse of near-wall acoustic bubbles, the micro-jet is gradually generated inside the cavitation bubble. The shape and size of cavitation bubble changes with the motion of bubbles and are related to the dimensionless parameter, γ, and the scale of bubbles [40]. In addition, the velocity of micro-jets also depends on the parameter, γ, and the maximum velocity of micro-jets occurs when γ is about 0.6–0.75 [41]. Using high-speed photography, Fig. 6 shows the size of cavitation bubbles generated by the ultrasonic vibratory device in Fig. 3 when γ is about 0.6–0.75. The results demonstrate the maximum diameter of bubbles can be approximately 409 μm. Therefore, the shape of micro-jets, when γ is about 0.6–0.75, is adopted in the study. Also, the detailed size and velocity are determined based on the results in Fig. 3 and relevant literature. Fig. 7 shows the model of 100 μm and 10 μm micro-jets with velocities of 600 m/s and 800 m/s. The friction coefficient of the contact surface is 0.1, and the calculation parameters are shown in Table 1. The concrete damage plasticity (CDP) model [42,43] is adopted to characterize the nonlinear behavior of concrete under impact loading [44], and the parameters are shown in Table 2 [45].

3.1.2. Results and analysis

Fig. 8 shows the node stress at the center of the impact loading ($v = 800$ m/s). The variation trends of stress curves of different nodes at the center match closely, and they are similar to the form of the proposed equivalent loading. However, the pressures at different positions in the action range of the micro-jet are different due to the shape of the micro-jet (Fig. 9). As seen in Fig. 9, the instantaneous hammer pressure is about 1.3 GPa, which is of a similar order of magnitudes to the calculation values in the literature [46–48].

The equivalent loadings at Points A, E, and F with $v = 800$ m/s are given in Fig. 10. As shown in Fig. 10, the loading on the impact center is larger than that on both sides. Furthermore, the center at both sides shows obvious characteristics of attenuation, indicating that the form of the equivalent loading is reasonable. These results are consistent with the previous analysis.

The indices of the average relative error, δ, and the mean square error (MSE) are adopted to verify the accuracy of the method. These indices can be calculated from the following:

$$\delta = \frac{|y_i - \widehat{y}_i|}{y_i} \times 100\% \quad (14)$$

$$MSE = \sqrt{\frac{\sum_{i=1}^{n}(y_i - \widehat{y}_i)^2}{n}} \quad (15)$$

In Eqs. (14)–(15), y_i is the simulated value using the CEL method, $\widehat{y}_i$ is the calculated value using the equivalent loading, and n is the number of selected points.

The comparison of deformation results for concrete under the action of the micro-jet against the equivalent loading are shown in Fig. 11. The average relative error and MSE are shown in Table 3. The simulated deformation based on the equivalent loading agrees well with the deformation obtained by the micro-jet method as seen by their similar magnitudes. Using the proposed equivalent loading method, the average relative errors range from 3.41% to 4.91%, and the MSEs range from 4.65×10^{-5} mm to 7.08×10^{-4} mm. The results demonstrate the proposed equivalent loading method improves the calculation efficiency while ensuring high simulation accuracy. As a whole, this provides technical support for subsequent multiple micro-jets simulations and macro-efficient simulation of cavitation damage.

With regard to near-wall acoustic bubble collapse micro-jet in the three-dimensional space, the impact of a jet is characterized as a typical axisymmetric problem, with the model and results given in Fig. 12. The displacement of concrete in the three-dimensional space is approximately symmetrical via a radial distribution. This displacement implies the pressures induced by a bubble collapse are not spread uniformly everywhere on the surface of the specimen, which agrees with previous results [49].

The displacement of any section is consistent with the two-dimensional calculation results. Therefore, the form of equivalent loading in the three-dimensional space is determined, the form of equivalent loading at any position is an impact loading, and the value of impact loading can be determined based on the equivalent loading of a two-dimensional model with high accuracy.

3.2. Multiple acoustic bubbles collapse

3.2.1. Model and parameters

Verifying the accuracy of multiple micro-jet collapses began with adopting a two-dimensional finite element generalization model of 0.5 mm × 20 mm (length × width). Next, the micro-jet velocity is assumed to be constant at a value of 800 m/s. According to the related research results, the number of micro-jets in the model is 5–50 [35], and the other parameters are shown in Tables 1 and 2.

3.2.2. Results and analysis

Figs. 13–15 show the deformation comparison results under the equivalent loading with a different number of micro-jets, the deformation cloud chart of concrete under multiple micro-jets, and the error results of two methods. The equivalent loading of the impact of multiple micro-jets has a strong correlation with the number of micro-jets, and the peak value, P_a, positively correlated with the number of micro-jets. Eq. (16) approximates the correlation as follows:

$$P_a = 45.859N \quad (16)$$

where N is the number of micro-jets.

Additionally, as seen in Figs. 14 and 15, the deformation of concrete under the uniform action of multiple micro-jets correlates to the number of micro-jets. Figs. 14 and 15 also display how the deformation at different positions is approximately uniform. The average relative errors at different positions using the two methods are less than 8%, and the maximum relative errors between the mean value of the two methods are less than 4%. The MSEs of $N = 30$ and $N = 50$ are 6.37×10^{-3} mm and 6.78×10^{-3} mm, respectively. The results imply that the equivalent loading method for multiple micro-jets has high accuracy and greatly improved efficiency.

4. Conclusions

In this study, the micro-jet theory is introduced to study the

equivalent method of the impact loading of cavitation erosion damage. Then, the collapse process of a single cavitation bubble can be approximately described by the high-speed impact of a specific shape micro-jet.

Based on the impact loading form of acoustic bubble collapse micro-jets determined by the water hammer pressure, an equivalent method of impact loading of a single acoustic bubble collapse micro-jet is established using the CEL method. In this method, the loading value varies with the position within the action range of the micro-jet.

Building upon the equivalent loading of a single acoustic bubble collapse micro-jet, the impact loading of multiple acoustic bubble collapse micro-jets in a micro-segment of the two-dimensional space can be modeled by a uniformly distributed impact load. This is made possible by assuming the acoustic bubbles are considered to be uniformly distributed in a small enough area. Based on this, the equivalent method of impact loading of multiple acoustic bubble collapse micro-jets is derived and proposed.

The results show the cavitation behavior of concrete under equivalent loading is consistent with that of a micro-jet simulation, and the average relative errors are about 3.41–8%, supporting the accuracy of the proposed method. This work provides a preliminary method for the numerical simulation of cavitation erosion of materials.

CRediT authorship contribution statement

Xiang Lu: Conceptualization, Methodology, Writing - original draft. **Chen Chen:** Investigation, Supervision, Writing - review & editing. **Kai Dong:** Software, Visualization. **Zefa Li:** Data curation, Software. **Jiankang Chen:** Supervision, Writing - review & editing.

Declaration of Competing Interest

The authors declare that they have no known competing financial interests or personal relationships that could have appeared to influence the work reported in this paper.

Acknowledgments

References

[1] M. Dular, A. Osterman, Pit clustering in cavitation erosion, Wear 265 (2008) 811–820, https://doi.org/10.1016/j.wear.2008.01.005.

[2] J. Luo, W. Xu, Y. Zhai, Q. Zhang, Experimental study on the mesoscale causes of the influence of viscosity on material erosion in a cavitation field, Ultrasonics Sonochemistry 59 (2019), 104699, https://doi.org/10.1016/j.ultsonch.2019.104699.

[3] L. Ye, X. Zhu, Y. He, X. Wei, Ultrasonic cavitation damage characteristics of materials and a prediction model of cavitation impact load based on size effect, Ultrasonics Sonochemistry 66 (2020), 105115, https://doi.org/10.1016/j.ultsonch.2020.105115.

[4] W. Xu, J. Li, Y. Zhai, J. Luo, H. Wu, J. Deng, Influence of multiple air bubbles on the collapse strength of a cavitation bubble, Experimental Thermal and Fluid Science 123 (2021), 110328, https://doi.org/10.1016/j.expthermflusci.2020.110328.

[5] J. Luo, W. Xu, B. Khoo, Stratification effect of air bubble on the shock wave from the collapse of the cavitation bubble, Journal of Fluid Mechanics 919 (2021) A16, https://doi.org/10.1017/jfm.2021.368.

[6] J.R. Laguna-Camacho, R. Lewis, M. Vite-Torres, J.V. Méndez-Méndez, A study of cavitation erosion on engineering materials, Wear 301 (1-2) (2013) 467–476, https://doi.org/10.1016/j.wear.2012.11.026.

[7] P. Cui, Q.X. Wang, S.P. Wang, A.M. Zhang, Experimental study on interaction and coalescence of synchronized multiple bubbles, Physics of Fluids 28 (1) (2016) 012103, https://doi.org/10.1063/1.4939007.

[8] A. Philipp, W. Lauterborn, Cavitation erosion by single laser-produced bubbles, Journal of Fluid Mechanics 361 (1998) 75–116, https://doi.org/10.1017/S0022112098008738.

[9] Y. Pan, F. Ma, B. Liu, T. Cai, Cavitation intensity and erosion pattern of a self-excited cavitating jet, Journal of Materials Processing Technology 282 (2020), 116668, https://doi.org/10.1016/j.jmatprotec.2020.116668.

[10] E, M., Hu, H., Guo, X., Zheng, Y. Comparison of the cavitation erosion and slurry erosion behavior of cobalt-based and nickel-based coatings. Wear, 428-429 (2019) 246-257. 10.1016/j.wear.2019.03.022.

[11] F. Alturki, A. Abouel-Kasem, S. Ahmed, Characteristics of cavitation erosion using image processing techniques, Journal of Tribology 135 (2013), 014502, https://doi.org/10.1115/1.4007575.

[12] Jing Zhang, Lingxin Zhang, Jian Deng, Numerical study of the collapse of multiple bubbles and the energy conversion during bubble collapse, Water 11 (2) (2019) 247, https://doi.org/10.3390/w11020247.

[13] L. Han, M. Zhang, G. Huang, B. Huang, Energy transformation mechanism of a gas bubble collapse in the free-field, Chinese Journal of Theoretical and Applied Mechanics 53 (2021) 1288–1301, https://doi.org/10.6052/0459-1879-21-006.

[14] A. Peters, O. Moctar, Numerical assessment of cavitation-induced erosion using a multi-scale Euler-Lagrange method, Journal of Fluid Mechanics 894 (2020) A19, https://doi.org/10.1017/jfm.2020.273.

[15] O. Usta, E. Korkut, Prediction of cavitation development and cavitation erosion on hydrofoils and propellers by Detached Eddy Simulation, Ocean Engineering 191 (2019), 106512, https://doi.org/10.1016/j.oceaneng.2019.106512.

[16] W. Lauterborn, H. Bolle, Experimental investigations of cavitation bubble collapse in the neighborhood of a solid boundary, Journal of Fluid Mechanics 72 (1975) 391–399, https://doi.org/10.1017/S0022112075003448.

[17] C. Kling, F. Hammitt, A photograph study of spark induce cavitation bubble collapse, Journal of Basic Engineering 94 (1972) 532–825, https://doi.org/10.1115/1.3425571.

[18] L. Ye, X. Zhu, Analysis of the effect of impact of near-wall acoustic bubble collapse micro-jet on Al 1060, Ultrasonics Sonochemistry 36 (2017) 507–516, https://doi.org/10.1016/j.ultsonch.2016.12.030.

[19] Feng, H., Huang, H., Li, Q., Shi, C. Wind-induced vibration time history analysis and equivalent static wind loads for long-span lattice shells. Journal of Vibration and Shock, 35 (2016) 164-173. 10.13465/j.cnki.jvs.2016.01.027.

[20] B. Oh, S. Jeon, Limitations and realistic application of equivalent load methods in pre-stressed concrete structures, Magazine of Concrete Research 54 (2002) 223–231, https://doi.org/10.1680/macr.54.3.223.38796.

[21] S. Wang, Y. Li, L. Zhang, A. Li, Y. Deng, Study on the equivalent method of the live load of urban transportation hub floor slab, Building Structure 49 (2019) 65–71.

[22] D. Wu, Y. Wu, J. Zhang, Multi-objective equivalent static wind loads for large span roofs, Journal of Building Structures 32 (2011) 17–23, https://doi.org/10.1631/jzus.B1000185.

[23] Y. Zhang, G. Yang, H. Hu, Y. Wen, Y. Jiang, P. Liu, J. Yao, Study on numerical model and safety criterion of the influence of blasting vibration on buildings and structures, China Civil Engineering Journal 48 (2015) 22–29.

[24] R. Dong, Y. Ge, Y. Yang, J. Wei, Multi-target equivalent static wind loads of long-span bridges based on proper orthogonal modes, China Civil Engineering Journal 52 (2019) 110–117.

[25] R. Gao, J. Li, Equivalent constant-amplitude fatigue load method based on the energy equivalence principle, Advances in Structural Engineering 22 (2019) 2892–2906, https://doi.org/10.1177/1369433219852705.

[26] C. Wang, H. Ding, H. Lv, Analysis on hydrodynamic load that induces high dam body vibration, Applied Mechanics and Materials 580–583 (2014) 1812–1815, https://doi.org/10.4028/www.scientific.net/AMM.580-583.1812.

[27] J. Chen, L. Zhang, Y. Chen, B. Yang, Z. Ding, Equivalent method for simulating uplift pressure in dam model test, Advances in Structural Engineering 13 (2010) 1063–1073, https://doi.org/10.1260/1369-4332.13.6.1063.

[28] W.F. Noh, CEL: A time-dependent, two-space-dimensional, coupled Eulerian-Lagrangian code, Academic Press, New York, NY, US, 1964, pp. 117–179.

[29] J.H. Lee, M.J. Youn, A new improved continuous variable structure controller for accurately prescribed tracking control of BLDD servo motors, Automatica 40 (2004) 2069–2074, https://doi.org/10.1016/j.automatica.2004.06.010.

[30] Cook, S.S. Erosion by water-hammer. Proceedings of the Royal Society of London, Series A. 119 (1928) 481-488. 10.1098/rspa.1928.0107.

[31] M. Plesset, R. Chapman, Collapse of an initially spherical vapour cavity in the neighborhood of a solid boundary, Journal of Fluid Mechanics 47 (1971) 283–290, https://doi.org/10.1017/S0022112071001058.

[32] F.J. Heymann, High-speed impact between a liquid drop and a solid surface, Journal of Applied Physics 40 (1969) 5113–5122, https://doi.org/10.1063/1.1657361.

[33] Ye, L., Zhu, X., Wang, J., Zhang, L. Simulations of ultrasonic cavitation micro-jet impact with different angles based on CEL. Journal of Vibration and Shock, 35 (2016) 130-134+157. 10.13465/j.cnki.jvs.2016.16.021.

[34] Z. Xie, W. Shi, Y. Zheng, L. Tan, Q. Tian, Y. Cao, J. Zhou, X. Ge, Simulation investigation on impact damage characteristics of metal plate by cavitating bubble micro-jet water hammer, Engineering Failure Analysis 115 (2020), 104626, https://doi.org/10.1016/j.engfailanal.2020.104626.

[35] F.G. Hammit, Cavitation and multiphase flow phenomena, Mc Graw -Hill Book Co, New York, 1980.

[36] A. Moussatov, C. Granger, B. Dubus, Cone-like bubble formation in ultrasonic cavitation field, Ultrasonics Sonochemistry 10 (2013) 191–195, https://doi.org/10.1016/S1350-4177(02)00152-9.

[37] Tongji University Department of Applied Mathematics, Advanced Mathematics (Volume two), Higher Education Press, Beijing, 2005.

[38] Z. Li, Z. Wu, J. Chen, L. Pei, X. Lu, Fuzzy seismic fragility analysis of gravity dams considering spatial variability of material parameters, Soil Dynamics and

Earthquake Engineering 140 (2021), 106439, https://doi.org/10.1016/j.soildyn.2020.106439.

[39] Z. Li, Z. Wu, J. Chen, X. Lu, L. Pei, C. Chen, Effect of correlated random fields on nonlinear dynamic responses of gravity dam, Natural Hazards 106 (2021) 79–96, https://doi.org/10.1007/s11069-020-04451-5.

[40] O. Supponen, D. Obreschkow, M. Tinguely, P. Kobel, N. Dorsaz, M. Farhat, Scaling laws for jets of single cavitation bubbles, Journal of Fluid Mechanics 802 (2016) 263–293, https://doi.org/10.1017/jfm.2016.463.

[41] A. Vogel, E. Brujan, P. Schmidt, K. Nahen, Interaction of laser-produced cavitation bubbles with an elastic tissue model, Proceedings of SPIE 4257 (2001) 167–177, https://doi.org/10.1117/12.434701.

[42] J. Lubliner, J. Oliver, S. Oller, E. Oñate, A plastic-damage model for concrete, International Journal of Solids & Structures 25 (1989) 299–329, https://doi.org/10.1016/0020-7683(89)90050-4.

[43] J. Lee, G.L. Fenves, Plastic-damage model for cyclic loading of concrete structures, Journal of Engineering Mechanics 124 (1998) 892–900, https://doi.org/10.1061/(ASCE)0733-9399(1998)124:8(892).

[44] Y. Huan, Q. Fang, L. Chen, Y. Zhang, Evaluation of blast-resistant performance predicted by damaged plasticity model for concrete, Transactions of Tianjin University 14 (2008) 414–421, https://doi.org/10.1007/s12209-008-0071-1.

[45] X. Lu, Z.Y. Wu, L. Pei, K. He, J.K. Chen, Z.F. Li, Z. Yang, Effect of the spatial variability of strength parameters on the dynamic damage characteristics of gravity dams, Engineering Structures 183 (2019) 281–289, https://doi.org/10.1016/j.engstruct.2019.01.042.

[46] Y. Wang, B. Lebon, I. Tzanakis, Y. Zhao, K. Wang, J. Stella, T. Poirier, G. Darut, H. Liao, M. Planche, Experimental and numerical investigation of cavitation-induced erosion in thermal sprayed single splats, Ultrasonics Sonochemistry 52 (2019) 336–343, https://doi.org/10.1016/j.ultsonch.2018.12.008.

[47] Georges L. Chahine, Chao-Tsung Hsiao, Modelling cavitation erosion using fluid-material interaction simulations, Interface Focus 5 (5) (2015) 20150016, https://doi.org/10.1098/rsfs.2015.0016.

[48] G. Chahine, Pressures generated by a bubble cloud collapse, Chemical Engineering Communications 28 (1984) 355–367, https://doi.org/10.1080/00986448408940143.

[49] G. Fatjó, A. Pérez, T., Hadfield, M., Experimental study and analytical model of the cavitation ring region with small diameter ultrasonic horn, Ultrasonics Sonochemistry 18 (2011) 73–79, https://doi.org/10.1016/j.ultsonch.2009.12.006.